Tribology International 72 (2014) 131–142

Contents lists available at ScienceDirect

Tribology International

journal homepage: www.elsevier.com/locate/triboint

Moving textures: Simulation of a ring sliding on a textured liner

Hugo M. Checo [a,*], Roberto F. Ausas [a], Mohammed Jai [b], Jean-Paul Cadalen [c], Franck Choukroun [c], Gustavo C. Buscaglia [a]

[a] Inst. Ciências Matemáticas e de Computação, Univ. São Paulo, 13560-970 São Carlos, Brazil
[b] ICJ, INSA de Lyon (Pôle de Mathématiques), 69621 Villeurbanne, France
[c] RENAULT, 67, Rue des Bons Raisins, 92508 Rueil Malmaison, France

ARTICLE INFO

Article history:
Received 11 July 2013
Received in revised form
12 December 2013
Accepted 18 December 2013
Available online 25 December 2013

Keywords:
Piston ring
Hydrodynamic lubrication
Mass-conservative model
Pocketed surface

ABSTRACT

Numerical simulations of the ring/liner contact in which the liner exhibits a periodic texture (pockets) are reported. The mass-conservative Elrod–Adams model is used to treat cavitation, and the dynamics of the ring is considered with a linear mass that corresponds to actual engine compression rings. The results, computed at a Stribeck number of 10^{-3} and thus in the hydrodynamic lubrication regime, show that the ring profile determines whether pocketing is beneficial or not. For strongly non-conformal contacts pocketing is detrimental, but for quasi-conformal contacts friction reductions of up to 73% are predicted. The largest reduction in friction was obtained for textures consisting of close-packed arrays of circular pockets of diameter comparable to the size of the contact.

1. Introduction

Texturing of contact surfaces to reduce friction and wear has attracted much attention in the last years, especially since surface microengineering techniques have become available. One important application is the piston-ring/cylinder-liner contact in combustion engines, which accounts for about 5% of fuel consumption [1].

It is known that some texture is needed to avoid stiction between the ring pack and the liner, and honed liners have been used for many decades for that purpose. Current investigations are aimed at determining the best texture in terms of friction and wear for each working condition.

Numerical and experimental studies on the ring/liner lubrication problem with textured surfaces are recent and quite scarce.

The numerical studies have only considered the texture to be on the ring, and thus stationary with respect to the contact. Kligerman et al. [2] solved the problem for flat textured and partially textured rings using the Reynolds equation and Reynolds boundary condition, which is known not to conserve mass. They concluded that surface texture reduces the friction between the surfaces. On the other hand, Tomanik [3], with the same cavitation model, numerically compared barrel shaped rings (compression rings), flat rings (oil control rings) and flat partially textured rings, also incorporating experimental data in the analysis. His results (both numerical and experimental) showed that the untextured barrel-shaped rings performed better than their flat, partially textured counterparts, both in hydrodynamic support and in friction coefficient. This finding coincides with recent numerical results of Gadeschi et al. [4] assessing the effect of Laser Surface Texture (LST) pockets on barrel-shaped rings. These authors adopted the Reynolds equation with Gümbel boundary conditions, which are non mass-conservative.

The goal of this paper is to present numerical simulations of hydrodynamic ring/liner contact with a *mass-conservative cavitation model* and *considering the texture as being on the liner* and thus moving through the computational domain, as sketched in Fig. 1. Similar simulations have only been reported up to now by Yin et al. [5], though with Reynolds cavitation condition (non-mass conservative), and by Tanaka and Ichimaru [6], who considered purely transversal textures, rendering the geometry one-dimensional, and adopted Reynolds cavitation condition.

The crucial importance of mass-conserving boundary conditions at cavitation boundaries has been established by Ausas et al. [7] and confirmed by several authors, among them Zhang and Meng [8] who performed a careful comparison with experiments.

The importance of considering textured *liners*, instead of textured rings, arises from several practical considerations: (a) All actual cylinder liners are, in fact, textured in some way. (b) The wear of the liner is smaller, and more evenly distributed, than that of the ring; the texture can thus be designed with more confidence in that it will preserve its shape for long operating

* Corresponding author. Tel.: +55 16 9233 3043.
E-mail addresses: hugocheco@gmail.com (H.M. Checo), rfausas@gmail.com (R.F. Ausas), mohammed.jai@insa-lyon.fr (M. Jai), jean-paul.cadalen@renault.com (J.-P. Cadalen), franck.choukroun@renault.com (F. Choukroun), gustavo.buscaglia@gmail.com (G.C. Buscaglia).

0301-679X/$ - see front matter © 2013 Elsevier Ltd. All rights reserved.
http://dx.doi.org/10.1016/j.triboint.2013.12.013

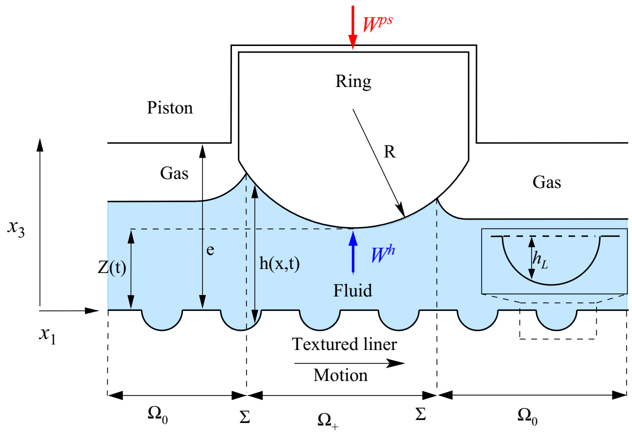

Fig. 1. Scheme of a section of the domain in the piston movement direction, with the forces acting on the ring.

times. (c) Since the rings contact the same axial position of the liner always at the same crank angle, texturing the liner allows one to optimize the texture that contacts the ring independently for each instant of the engine cycle.

The simulation of the ring/liner contact with texture on the liner also constitutes a scientific challenge from the numerical perspective. The dynamical behavior of the system is completely different depending on whether the texture is on the ring or on the liner. In the former case, the texture is stationary with respect to the contact, and thus the ring stabilizes at some position at which force equilibrium takes place. This position only changes with the time scale of variations in the relative velocity or oil-feeding conditions. If the texture is on the liner, the texture cells enter the contact from one side, move under the ring, and leave the contact at the opposite side. In this case the ring exhibits a superposed oscillatory motion with the time scale *per*/*u*, where *per* is the size of the texture cells and *u* the relative speed. The complexity grows substantially, since the simulation must be transient and must incorporate the rigid-body dynamics of the ring, which is subject to time-varying forces.

The simulations reported in this paper consider barrel-shaped rings in which the contact surface is cylindrical of radius *R*. Several values of *R* are considered, ranging from 2 mm to nominally conformal contact (*R* very large), so as to contribute to the interpretation of experimental findings.

Experimental studies of textured surfaces have mainly focused on conformal contacts (nominally flat pin or ring on nominally plane disk) [8–13]. Experiments in non-conformal contact configurations have yielded mixed results up to now. In a recent article, Kovalchenko et al. [14] found that dimpled disks accelerated the wear of the contacting ball and only as a result thereof some friction reduction could be attained. Their explanation focused on a change of regime from boundary to mixed lubrication. Ali et al. [15] performed ball-on-disk experiments and found that dents did not reduce friction in fully flooded conditions, whereas significant reduction was attained under severe starvation. Similar experiments by Li et al. [16] on PDMS disks lead them to conclude that texturing only reduces friction at low sliding velocities, consistent with a boundary or mixed lubrication regime. Other experimental studies of non-conformal contacts in the boundary lubrication regime have been reported by Kim et al. [17], Peterson and Jacobson [18,19]

The hydrodynamic lubrication regime was studied by Costa and Hutchins [20] by means of cylinder-on-plane experiments in which the texture was on the plane. For a cylinder diameter of 16 mm they found that all textured surfaces performed worse than the untextured one. For a cylinder diameter of 200 mm, on the other hand, they observed that the *average* film thickness, as measured by capacitance techniques, was improved by some non-zero textures. Unfortunately, they did not measure the *minimum* film thickness or the friction coefficient. Tomanik [21], on the other hand, used the compression ring of a heavy duty Diesel engine ($R \simeq 50$ mm) on several textured liners (pocketed and honed liners) and obtained that the untextured liner presented less friction than the textured ones. Some further information on the effect of the liner's striation patterns has been published by Grabon et al. [22] and by Yuan et al. [10], among others.

The plan of this paper is as follows: In Section 2 we describe the mathematical model, which is essentially based on the Elrod–Adams model for lubrication and cavitation [23]. Though the Elrod–Adams model has some deficiencies for this problem [24], there is no better general mass-conserving algorithm for cavitation problems [25]. Section 3 contains the numerical results. They correspond to fully flooded, hydrodynamic contact conditions at fixed relative velocity, and with atmospheric pressure (assumed equal to the cavitation pressure) on both sides of the ring. The texture is on the liner and its geometry corresponds to pockets inspired in those produced by Laser Surface Texturing (LST) [26], with depth, diameter and area density in the range of those recommended in LST applications. The mass assigned to the ring is typical of compression rings of car engines. By exploring hundreds of cases, a picture of the effect of textures on ring/liner friction emerges in which texturing is beneficial only for rings with sufficiently large *R*. This picture coincides with the one recently put forward by Gadeschi et al. [4] for non-moving textures (texture on the ring) on the basis of a non-mass-conservative model. Conclusions are drawn in Section 4.

2. Modeling

2.1. Geometrical model

We consider a configuration in which a single ring is in contact with the liner. The surface of the liner is developed along the x_1–x_2 plane, x_1 being the axial direction (coincident with that of the motion) and x_2 the circumferential one. The curvature along x_2 is neglected.

It is assumed that the ring is only allowed to move along x_3, its position being parameterized by Z. The origin of Z is chosen so that $Z=0$ corresponds to the ring touching the x_1–x_2 plane. The ring profile, $h_U(x_1,x_2)$ satisfies $\min_{(x_1,x_2)} h_U(x_1,x_2)=0$ and is shown in Fig. 2. Its analytical expression is the one corresponding to an arc of circumference of radius R.

The liner is assumed to coincide with the x_1–x_2 plane ($x_3=0$) when it is smooth (untextured). In the textured case, it is given by

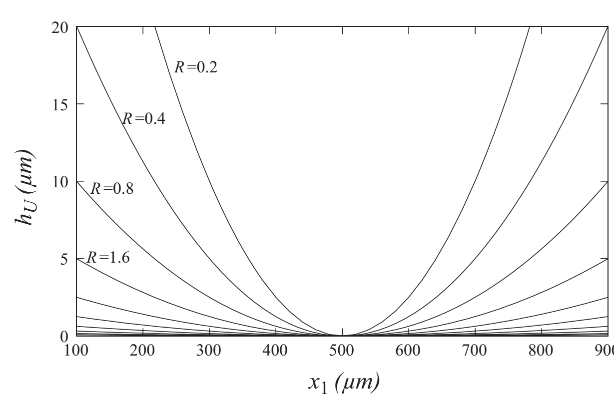

Fig. 2. Ring profiles for curvature radius ranging from R=0.2 to R=102.4 cm, in powers of 2.

some function $x_3 = -h_L(x_1, x_2) \le 0$. We consider here texture patterns inspired from LST surfaces (pocketed surfaces). Because of the arrangement of the pockets, the problem becomes periodic in x_2, so that in the simulation only one period is considered, $0 < x_2 < B$, with suitable boundary conditions at $x_2 = 0$ and $x_2 = B$.

The ring follows a uniform motion along x_1 with velocity $-u$. We adopt a frame of reference that moves with the ring, so that the velocity of the lower surface (liner) becomes u and the x_1-location of the ring is fixed between $x_1 = a$ and $x_1 = b$. Outside of the ring's position the gap between the surfaces is assumed to be uniform of thickness e (notice that this implies, in particular, that the ring axis is centered and aligned with the cylinder, which constitutes of course an idealization).

Under the assumptions above, the gap between the ring and the liner is given by

$$h(x_1, x_2, t) = \begin{cases} h_L(x_1 - u\,t, x_2) + h_U(x_1, x_2) + Z(t) & \text{if } a < x_1 < b \\ h_L(x_1 - u\,t, x_2) + e & \text{otherwise} \end{cases} \tag{1}$$

2.2. Forces on the ring

The dynamics of the ring is governed by the forces acting on it along the x_3-direction. These forces are described below.

The *pre-stress force* comes from the elastic response of the ring to the deformation needed to make it fit into its placement. It points outwards (i.e., along $-x_3$) and can be assumed constant. We denote by W^{ps} its value *per unit length along* x_2.

The *hydrodynamic force* originates from the pressure $p(x_1, x_2, t)$ that develops in the oil film between the ring and the liner. Its value per unit length along x_2 is given by

$$W^h(t) = \frac{1}{B} \int_a^b \int_0^B p(x_1, x_2, t)\, dx_1\, dx_2 \tag{2}$$

The pressure field p comes out from the hydrodynamic model that is described in the next subsection.

From the above considerations, if m is the mass of the ring per unit length, then the dynamical equation for the ring's displacement reads as

$$m\frac{d^2 Z}{dt^2} = W^{ps}(t) + W^h(t) \tag{3}$$

This is supplemented with initial conditions for Z and Z' at $t=0$. For the model to be in closed form it only remains to explain the calculation of the hydrodynamic pressure p.

2.3. Hydrodynamics and cavitation modeling

We adopt here the well-known Elrod–Adams model [23], which incorporates into a single formulation Reynolds equation for the pressurized region and Jacobsson–Floberg–Olsson boundary conditions. This model is mass conserving, which as shown by [7] is essential for obtaining physically meaningful results in lubrication problems involving textured surfaces.

The model postulates the computation of two fields, p and θ, which correspond to the hydrodynamic pressure and to an auxiliary saturation-like variable, respectively, which (weakly) satisfy the equation

$$\nabla \cdot \left(\frac{h^3}{12\mu} \nabla p \right) = \frac{u(t)}{2} \frac{\partial\, h\theta}{\partial x_1} + \frac{\partial\, h\theta}{\partial t} \tag{4}$$

under the complementarity conditions:

$$\begin{cases} p > 0 \Rightarrow \theta = 1 \\ \theta < 1 \Rightarrow p = 0 \\ 0 \le \theta \le 1 \end{cases} \tag{5}$$

where μ is the viscosity of oil.

This model has been analyzed to a great extent by [27,28], and it has been shown to lead to well-posed problems in several physically meaningful situations. For the piston ring/liner contact we assume that the oil-film thickness is known (and constant, equal to d_{oil}) far away from the ring assembly. This amounts to imposing that $\theta = d_{oil}/h$ at the boundary of the computational domain. More precisely, if the computational domain corresponds to $x_{1\ell} < x_1 < x_{1r}$, then assuming $u > 0$ we impose $\theta(x_{1\ell}, x_2, t) = d_{oil}/h(x_{1\ell}, x_2, t)$. As already said, the boundary conditions along $x_2 = 0$ and $x_2 = B$ are defined so as to enforce the proper periodicity in that direction. An initial condition for θ is also provided.

As a consequence of the previous model, at each instant the domain spontaneously divides into a pressurized region, Ω^+, where $p > 0$, and a cavitated region, Ω^0, where the film is not full ($\theta < 1$, see Fig. 1). At the boundary between Ω^+ and Ω^0, the so-called cavitation boundary Σ, the Elrod–Adams model automatically enforces the mass-conservation condition:

$$\frac{h^3}{12\mu} \nabla p \cdot \hat{n} = \frac{u}{2}(1-\theta) h \hat{n} \cdot \hat{\imath} \tag{6}$$

where $\hat{n}$ is the normal to Σ (oriented outwards from Ω^0) and $\hat{\imath}$ is the unit vector along x_1. In particular, the saturation field θ turns out to be discontinuous at those parts of Σ where $u\,\hat{n} \cdot \hat{\imath}$ is positive (reformation boundary).

If the gap thickness h is discontinuous at the cavitation boundary, which is often the case in the textured case, Eq. (6) does not hold. However, the Elrod–Adams model considered as a conservation law $\partial_t \varphi + \nabla \cdot J = 0$, with $\varphi = h\theta$, remains in general well-posed and provides a physically meaningful solution (the theory is somewhat fragmented and does not cover all possible conditions, but sufficient evidence exists to safely assume well-posedness under initial and boundary conditions that make physical sense).

2.4. Friction losses

The friction force per unit width is given by

$$F = -\frac{1}{B} \int_a^b \int_0^B \left(\frac{\mu u\, g(\theta)}{h} + \frac{1}{2} h \frac{\partial p}{\partial x_1} + p \frac{\partial h_L}{\partial x_1} \right) dx_1\, dx_2 \tag{7}$$

where the function $g(\theta)$ is taken as

$$g(\theta) = \theta\, s(\theta) \tag{8}$$

with $s(\theta)$ is the switch function:

$$s(\theta) = \begin{cases} 1 & \text{if } \theta > \theta_s \\ 0 & \text{otherwise} \end{cases} \tag{9}$$

In this friction model θ_s is a threshold for the onset of friction, interpreted as the minimum oil fraction for shear forces to be transmitted from one surface to the other. In most of the calculations the value $\theta_s = 0.95$ has been adopted. Notice that h_L corresponds to the texture depth at each location, which changes with time as the texture moves below the ring. All oil films obtained in the simulations are thick enough to exclude the possibility of contact between the lubricated surfaces, so that solid–solid friction is not considered.

The friction coefficient then results from

$$f = \frac{-F}{W^{ps}} \tag{10}$$

Remark: The term $p\partial h_L/\partial x_1$ is not a shear force. Instead, it corresponds to the projection of the pressure force along x_1 when the normal to the liner is not along x_3. Since the liner is moving to the right, $\partial h_L/\partial x_1 > 0$ corresponds to a converging wedge which will produce a pressure force with a negative x_1 component, thus opposing the motion. Similarly, $\partial h_L/\partial x_1 < 0$ corresponds to a diverging wedge which will produce a pressure force with a positive x_1 component, thus assisting the motion. Since in general the pressure in converging wedges is higher than in diverging ones, this term is always negative and thus *always contributes positively to the friction*. Notice that this term is omitted in the literature, which mostly considers textures on the stationary surface.

2.5. Adimensionalization and final equations

We consider an adimensionalization of the equations based on the following fundamental scales:

Quantity	Scale	Scale value adopted
Velocity	U	10 m/s
Length	L	1 cm
Gap thickness	H	1 μm

These scales, together with the viscosity of the oil, assumed to be $\mu = 0.004$ Pa s lead to the following derived scales for the different quantities:

Quantity	Scale	Scale value	Name
x_1, x_2	L	10^{-2} m	
R	L	10^{-2} m	Ring profile curvature radius
t	$\frac{L}{U}$	10^{-3} s	Time
h	H	10^{-6} m	Gap thickness
Z	H	10^{-6} m	Ring's radial position
p	$\frac{6\mu UL}{H^2}$	2.4×10^9 Pa	Pressure
W^{ps}, W^h	$\frac{6\mu UL^2}{H^2}$	2.4×10^7 N/m	Radial forces per unit width
F	$\frac{\mu UL}{H}$	4×10^2 N/m	Friction force per unit width
m	$\frac{6L^4\mu}{H^3 U}$	2.4×10^7 kg/m	Mass per unit width

Notice that, since the scales for radial and friction forces are different, the friction coefficient is given by

$$f = \frac{H}{6L}\frac{\hat{F}}{\hat{W}^{ps}} \tag{11}$$

where the carets (hats) denote the corresponding non-dimensional quantity.

Upon adimensionalization of all variables, and omitting all carets for simplicity, let us collect the complete mathematical problem to be solved:

Find trajectory $Z(t)$, and fields $p(t)$, $\theta(t)$, defined on $\Omega = (x_{1\ell}, x_{1r}) \times (0, B)$ and periodic in x_2, satisfying

$$\begin{cases} Z(0) = Z_0, & Z'(0) = V_0, \\ \theta(x_{1\ell}, x_2, t) = d_{\mathrm{oil}}/h(x_{1\ell}, x_2, t) & \forall x_2 \in (0, B) \\ p > 0 \Rightarrow \theta = 1 \\ \theta < 1 \Rightarrow p = 0 \\ 0 \le \theta \le 1 \end{cases} \tag{12}$$

and

$$m\frac{d^2 Z}{dt^2} = W^{ps}(t) + W^h(t) \tag{13}$$

$$\nabla \cdot (h^3 \nabla p) = \frac{u}{2}\frac{\partial h\theta}{\partial x_1} + \frac{\partial h\theta}{\partial t} \tag{14}$$

where

$$h(x_1, x_2, t) = \begin{cases} h_L(x_1 - u\,t, x_2) + h_U(x_1, x_2) + Z(t) & \text{if } a < x_1 < b \\ h_L(x_1 - u\,t, x_2) + e & \text{otherwise,} \end{cases} \tag{15}$$

$$W^h(t) = \frac{1}{B}\int_a^b \int_0^B p(x_1, x_2, t)\, dx_1\, dx_2, \tag{16}$$

and the functions $W^{ps}(t)$, $h_L(x_1, x_2)$, $h_U(x_1, x_2)$ are known explicitly.

The formula for the adimensional friction force per unit width is

$$F = \frac{1}{B}\int_a^b \int_0^B \left(\frac{\mu u\, g(\theta)}{h} + 3h\frac{\partial p}{\partial x_1} + 6p\frac{\partial h_L}{\partial x_1}\right) dx_1\, dx_2 \tag{17}$$

It is thus composed of three terms, which are usually called (in order) Couette term, Poiseuille term and Pressure term.

2.6. Numerics

The numerical treatment is exactly as described in [29]. It consists of a finite volume, conservative method with upwinding discretization of the Couette flux and centered discretization of the Poiseuille flux and an iterative imposition of the cavitation conditions by means of a Gauss–Seidel-type algorithm. The dynamical equation for $Z(t)$ is discretized by a Newmark scheme, which is built into the overall iterative process. The simulations would not have been possible without significant acceleration obtained from multigrid techniques [30].

3. Numerical simulations

3.1. Preliminaries and definitions

The performance of the different contacts under study is assessed at conditions of low applied load, corresponding to a Stribeck parameter of 10^{-3}. The Stribeck parameter S is defined by

$$S = \frac{\mu\, u}{W^{ps}} \tag{18}$$

where μ, u and W^{ps} are dimensional. In terms of the non-dimensional variables used in the code, the expression is (here we temporarily put carets on non-dimensional variables to avoid confusion, but they are dropped hereafter)

$$S = \frac{H^2}{6L^2}\frac{\hat{u}}{\hat{W}^{ps}} \tag{19}$$

For any value of S, the friction factor f is a function of time, since it changes as the textures change position under the ring. However, since the studied textures are periodic, f reaches a periodic regime after a few passages of individual textures (see Fig. 5 for a concrete example). So does the ring position Z and, as a consequence, the minimum clearance C between the surfaces.

In our assessment, the *average* friction coefficient $\overline{f}$ is used to quantify friction, where the average is performed over one period of the motion once the ring has attained the periodic regime. To quantify wear, on the other hand, we report the *minimum* clearance $C_{\min}$, defined as the minimal separation between the surfaces over the period.

3.2. Pocketed surfaces

We consider surfaces exhibiting dimples with the contour of an ellipse (see Fig. 3), with the ellipse semiaxis l_1 oriented along the piston movement direction and l_2 orthogonal to it. The dimples′centers are separated by distances *per* and *width* along these directions. In the cases under study the dimples are arranged in a square motif (*per*=*width*). We consider dimples that have the shape of half an ellipsoid of semiaxis *prof* orthogonal to the liner surface.

3.3. Mesh convergence

A mesh convergence study is needed to prove the soundness of the numerical method under moving-texture conditions. Consider the case of a pocketed liner with parameters $per=0.06$, $l_1=0.01$, $l_2=0.01$, $prof=5.0$, $u=1.0$ and $W^{ps}=1.66\times10^{-6}$, corresponding to $S=10^{-3}$, with a linear ring mass of 2.0×10^{-9} (which is a realistic value). The simulation starts with the ring separated 2.5 μm from the liner′s plateau ($Z(0)=2.5$), with zero velocity ($Z'(0)=0$). The domain is 0.2 cm in the axial direction (x_1) and 300 μm along x_2 (just half the domain is simulated, with reflection boundary conditions).

A 512×32 spatial mesh is considered as a starting point for the refinement, with time step $\delta t=4\times10^{-4}$, for 1.6 s of simulation. The refined meshes have 1024×64 cells (run with $\delta t=2\times10^{-4}$) and 2048×128 cells (run with $\delta t=10^{-4}$). Fully flooded conditions are taken (fluid film of 20 μm imposed at the left boundary).

Fig. 4 shows the position x_1 of the cavitation boundary along the line $x_2=per/2$ (corresponding to the longitudinal line passing through the dimples′ centers) as a function of time. Though the cavitation boundary is a very sensitive variable, it can be seen that its position for each time converges steadily (with roughly first order in the mesh size).

Let us now turn to the convergence of the friction force, since it will be the focus of the results in the next sections. In Fig. 5(b) the total friction force versus time, and a detail thereof, is shown. As mentioned, there is an adjustment period of about 1 time unit until the ring reaches its stable motion, which is periodic in time with period per/u. Convergence of the friction force is observed in the figure, both in the initial transient and in the periodic regime. The relative errors in the average friction force in the periodic regime on the meshes with 512×32 and 1024×64 cells, as compared to those computed on the 2048×128 mesh, are of 0.72% and 0.27%, respectively. The numerical errors for the computations made on the 512×32 mesh, therefore, can be estimated at 1%. It is this mesh that is employed in all the computations presented heretoforth, though some of them have been computed in all three meshes to check that the claimed conclusions are not consequences of numerical artifacts.

3.4. Effect of surface texturing on friction for different ring profiles

This study considers the cylindrical ring profiles shown in Fig. 2. The Stribeck number is fixed at $S=10^{-3}$ (hydrodynamic regime) and the inlet oil thickness chosen so as to yield fully flooded conditions ($d_{oil}=20$). The other parameters are $u=1$, $W^{ps}=1.66\times10^{-6}$, and a linear ring mass of 2.0×10^{-9}, as before. A range of the parameters that define the texture shape was explored, simulating for each texture shape the transient lubrication problem for 10 different ring shapes (non-dimensional curvature radii from $R=0.2$ to $R=102.4$). Specifically, all combinations of the values of the three parameters l_1 (pocket length, taken equal to its width l_2), *per* (texture-cell length, taken equal to its *width*) and *prof* (pocket depth) were computed for ten different values of R. This yields a total of $8\times6\times5\times10=2400$ cases. Excluding those combinations which are geometrically incompatible (because $2l_1>per$) and those which do not satisfy the thin film hypothesis (because $l_1<5\,prof$), there remain 720 cases:

$l_1=l_2$	Period	Depth
0.001	0.005	2
0.0025	0.005	5
0.005	0.01	10
0.01	0.02	20
0.02	0.03	30
0.03	0.04	
	0.05	
	0.06	

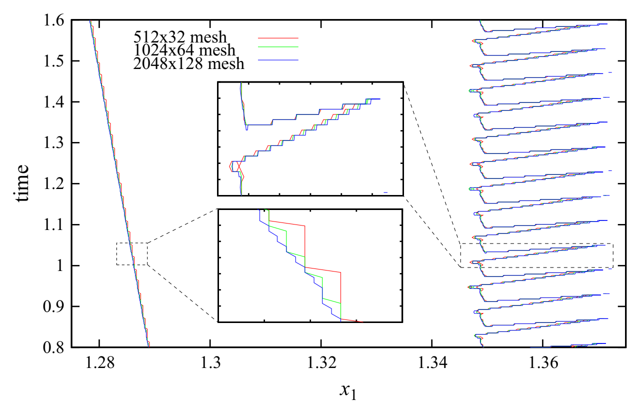

Fig. 4. Position x_1 of the cavitation boundaries on the line $x_2=per/2$, which passes through the dimples′ centers. Shown are the results for the 512×32, 1024×64 and 2048×128 meshes, exhibiting convergent behavior of first order.

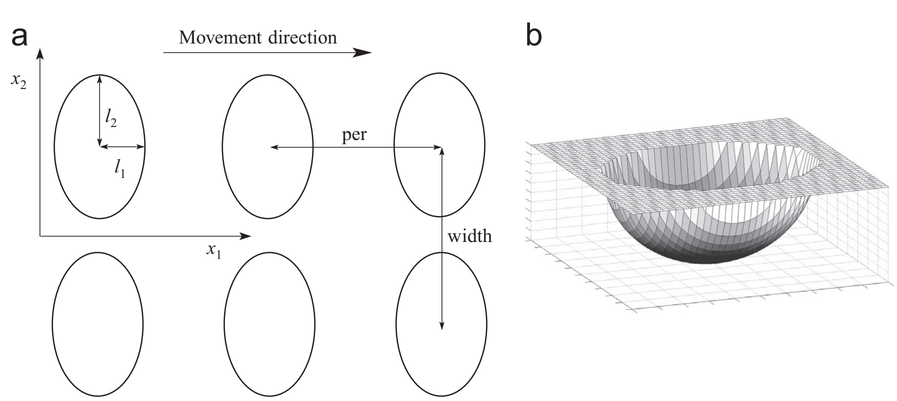

Fig. 3. (a) Pocketed texture and (b) Ellipsoidal-bottomed dimple.

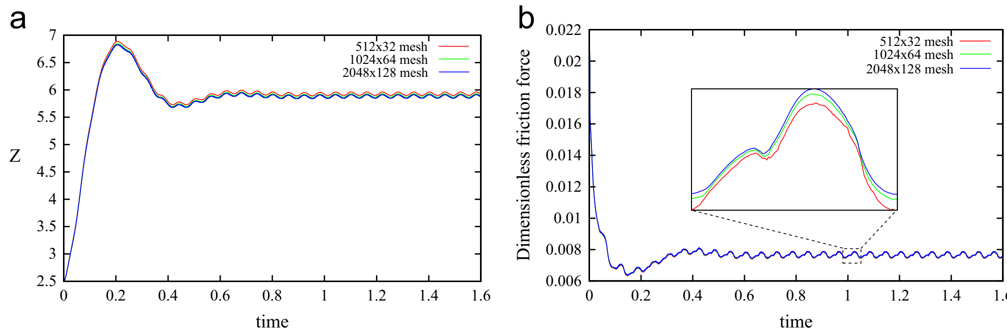

Fig. 5. (a) Piston position and (b) friction force in the x_1 direction for the 512×32, 1024×64 and 2048×128 meshes.

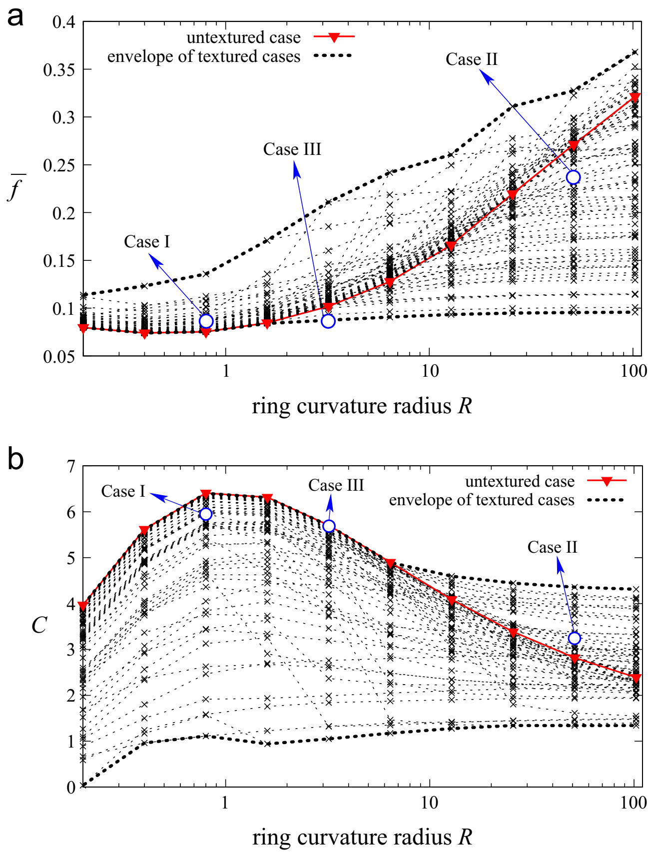

Fig. 6. All the 72 curves for (a) friction and (b) minimum clearance with the envelope of those and the untextured case ($S=1.0\times10^{-3}$).

Table 1
Tables showing the best textures in terms of the average friction coefficient (a) or of the minimum film thickness (b). For each criterion, the best five textures for rings with small R are shown on the left, while the best five for rings with large R are shown on the right.

Small R				Large R			
#	$l_1=l_2$	*per*	*prof*	#	$l_1=l_2$	*per*	*prof*
(a) Best textures in terms of friction							
1	0.0025	0.06	2	1	0.03	0.06	10
2	0.0025	0.05	2	2	0.03	0.06	5
3	0.0025	0.04	2	3	0.03	0.06	20
4	0.0025	0.03	2	4	0.02	0.04	10
5	0.005	0.06	2	5	0.02	0.04	5
(b) Best textures in terms of clearance							
1	0.0025	0.06	2	1	0.03	0.06	5
2	0.0025	0.05	2	2	0.02	0.05	5
3	0.0025	0.04	2	3	0.02	0.06	5
4	0.0025	0.06	5	4	0.03	0.06	10
5	0.0025	0.05	5	5	0.03	0.06	2

These cases were organized as 72 curves giving the average friction coefficient $\bar{f}$ and minimum clearance $C_{\min}$ of each texture as a function of the curvature radius of the ring. The curves are all plotted simultaneously in Fig. 6, in black dotted lines with a cross at each actual simulation result. The friction and clearance obtained with a perfectly flat liner (untextured) is displayed as a thick red line with a triangle indicating each actual simulation.

It is observed in Fig. 6 that none of the simulated textures attains lower friction than the untextured liners when $R<1.6$ (notice that this value corresponds to 1.6 cm). The lowest overall friction is obtained with a ring having $R=0.8$ sliding on an untextured liner. This configuration also maximizes the clearance between ring and liner. For flatter rings, those with $R=3.2$ or greater, there are textures that improve both the friction and the clearance.

One can thus divide the results into two general classes, corresponding to either small values of R or large values of R. For each class, one can find the textures that yield the lowest average friction (Table 1(a)) and those that yield the largest minimum clearance (Table 1(b)). The best liner for small-R rings is, as mentioned, one with untextured surface. Considering the explored ranges of l_1, *per* and *prof*, one observes that the lowest friction and largest clearance are obtained with the smallest values of l_1 and *prof*, together with the greatest values of *per*. In other words, the best textures correspond to liner surfaces as planar as possible.

The best liner for large-R rings, on the other hand, exhibits a non-zero texture with $l_1=l_2=0.03$, $per=0.06$ and $prof=10$ (or $prof=5$ if one wants the maximal clearance). This corresponds to pockets touching one another, i.e., dimple length and width equal to the texture-cell size.

To provide some insight into the detailed physics taking place during the passage of each texture cell under the ring, three cases are reported in detail in the next section. These cases are labeled Case I, Case II and Case III in Fig. 6. In fact, Case III corresponds to the texture that yields lowest friction for large-R rings.

Let us however insert a few comments before going into the detailed case analyses:

- The radius of curvature of actual piston compression rings is of about 5 cm [31], corresponding to $R=5$ and thus falling into the large-R class in which texturing the liner may be beneficial (at least for the Stribeck number considered here, $S=10^{-3}$).
- There could exist a width-to-length ratio l_2/l_1 that improves the friction for small-R rings. Though not illustrated here, we

explored other pocket shapes, with $l_2/l_1=0.25$, 0.5, 2 and 4, and none of them yielded better performances than circular pockets.

3.5. Analysis of three cases

Here we analyze and compare the following three cases:

- *Case* I: A textured liner with $l_1=l_2=0.01$, $per=0.06$ and $prof=5.0$, combined with a ring having $R=0.8$. In this configuration, the textured liner yields higher friction and lower clearance than the untextured one. The textured area fraction is 8.7%.
- *Case* II: The same textured liner ($l_1=l_2=0.01$, $per=0.06$ and $prof=5.0$) now combined with a large-R ring ($R=51.2$). In this configuration the texture is beneficial both in friction and in clearance. The textured area fraction is 8.7%.
- *Case* III: A textured liner with $l_1=l_2=0.03$, $per=0.06$ and $prof=10.0$, combined with a ring having $R=3.2$. This corresponds to the texture yielding the lowest friction for the given value of R. The textured area fraction is 78.5%.

In Fig. 7, the first line from the top (parts (a) and (b)) corresponds to Case I, while the second and third correspond to Cases II and III, respectively. The ring position is highest for Case I, being 6.41 (microns) above the liner if untextured and about 6.25 if textured. The corresponding friction coefficients are, accordingly, the lowest of the three cases (0.00754 for the untextured liner and 0.00763 for the textured one, remarkably similar considering that 8.7% of the area consists of pockets of depth 5 μ). One also observes that the friction is dominated by the Couette term, which is increased (in mean) by the texture. Fig. 8 shows the pressure profile and the film thickness at several instants along the passage of one individual pocket under the ring. At instants (c) to (f), the pressure generated under the ring is greater than the one generated on the untextured liner. The pocket creates additional lift, thus, when it is centered under the ring or slightly towards the diverging side of it (up to one pocket diameter to the right). At instants (h) to (a) the pocket is detrimental for pressure generation, corresponding to the pocket being upstream of the ring's apex. Notice that in Case I, since the contact is strongly non-conformal (small-R ring), the pressure field always exhibits a main pressurized region (positive p) on the left (converging) half of the ring.

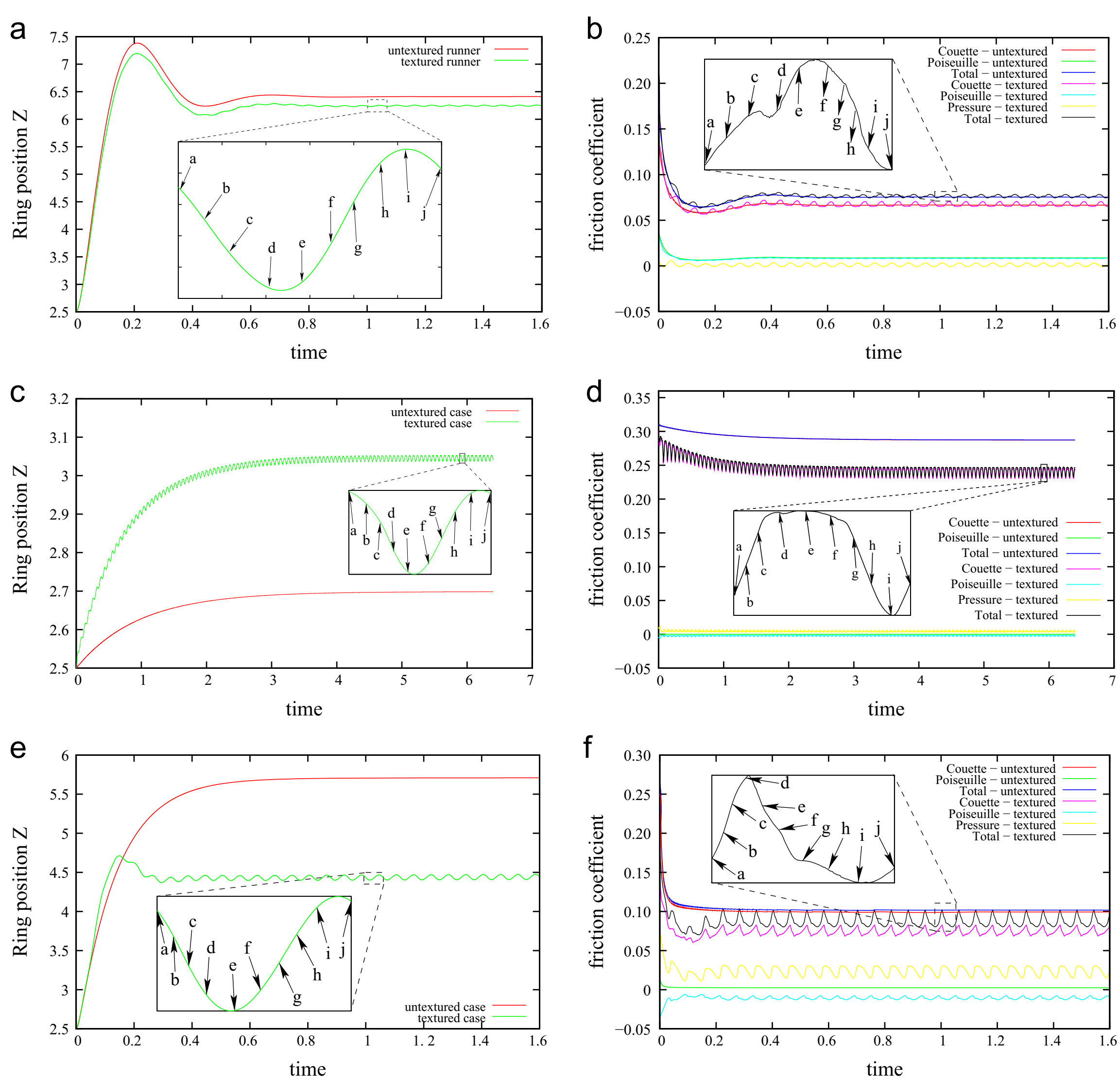

Fig. 7. Ring position Z (a, c, e) and instantaneous friction force terms (b, d, f) for Cases I–III. Points "a"–"j" in the inset of parts (a) and (b) correspond to the instants shown in Fig. 8 (Case I). Points "a"–"j" in the inset of parts (c) and (d) correspond to the instants shown in Fig. 9 (Case II). Points "a"–"j" in the inset of parts (e) and (f) correspond to the instants shown in Fig. 10 (Case III).

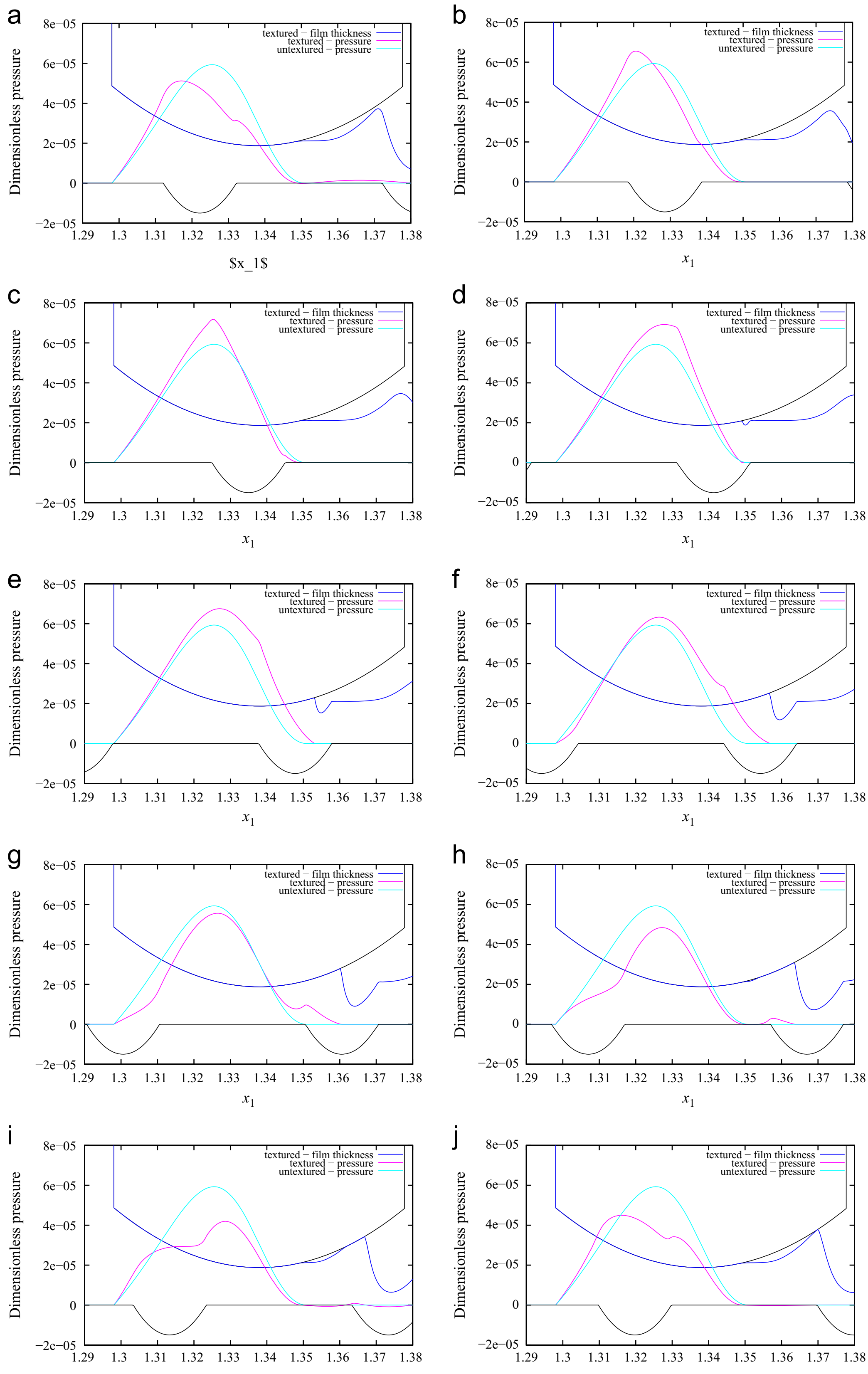

Fig. 8. Instantaneous pressure and film thickness profiles for Case I at times: (a) $t=0.9920$, (b) $t=0.9984$, (c) $t=1.0048$, (d) $t=1.0112$, (e) $t=1.0176$, (f) $t=1.0240$, (g) $t=1.0304$, (h) $t=1.0368$, (i) $t=1.0432$, (j) $t=1.0496$ (Points "a" through "j" in the insets of Fig. 7(a) and (b)).

Parts (c) and (d) of Fig. 7 show that for Case II the textured liner performs much better than the untextured one. There is a gain of 0.35 μ in the ring's position (from 2.70 to 3.05), and a 15.7% decrease in the friction coefficient (from 0.0287 to 0.0242). As in Case I, the friction is dominated by the Couette term in which this time is significantly *decreased* by the texture. The corresponding instantaneous profiles of pressure and film thickness are shown in Fig. 9. The contact in this case is conformal (large-R ring), and one observes that the main pressurization takes place at the left end of the pocket, irrespective of its position under the ring. Each pocket "carries" its own pressure field with it as it moves to the right. The lift force generated in this way pushes the ring further away

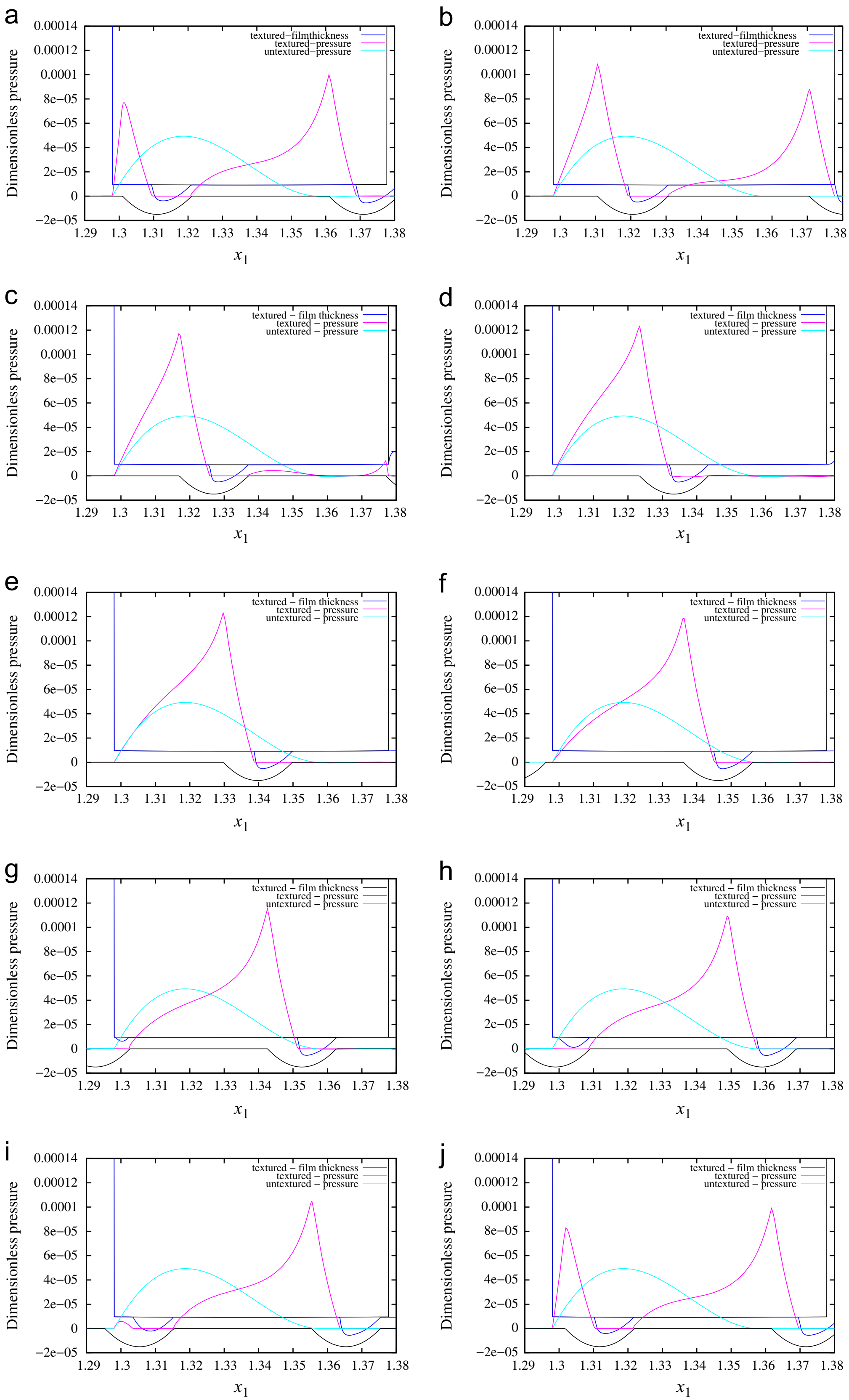

Fig. 9. Instantaneous pressure and film thickness profiles for Case II at times: (a) t=5.9008, (b) t=5.9104, (c) t=5.9168, (d) t=5.9232, (e) t=5.9296, (f) t=5.9360, (g) t=5.9424, (h) t=5.9488, (i) t=5.9552, (j) t=5.9616 (Points "a" through "j" in the insets of Fig. 7(c) and (d)).

from the liner, thus reducing the average friction force (dominated by the Couette term proportional to $1/h$).

Finally, the ring position and friction coefficient of Case III are plotted versus time in parts (e) and (f) of Fig. 7. This configuration exhibits some striking features. The textured liner produces a friction that is lower than that of the untextured one, but not, as in Case II, by lifting the ring farther away. In fact, the minimum clearance of the textured liner is 4.44, while that of the untextured

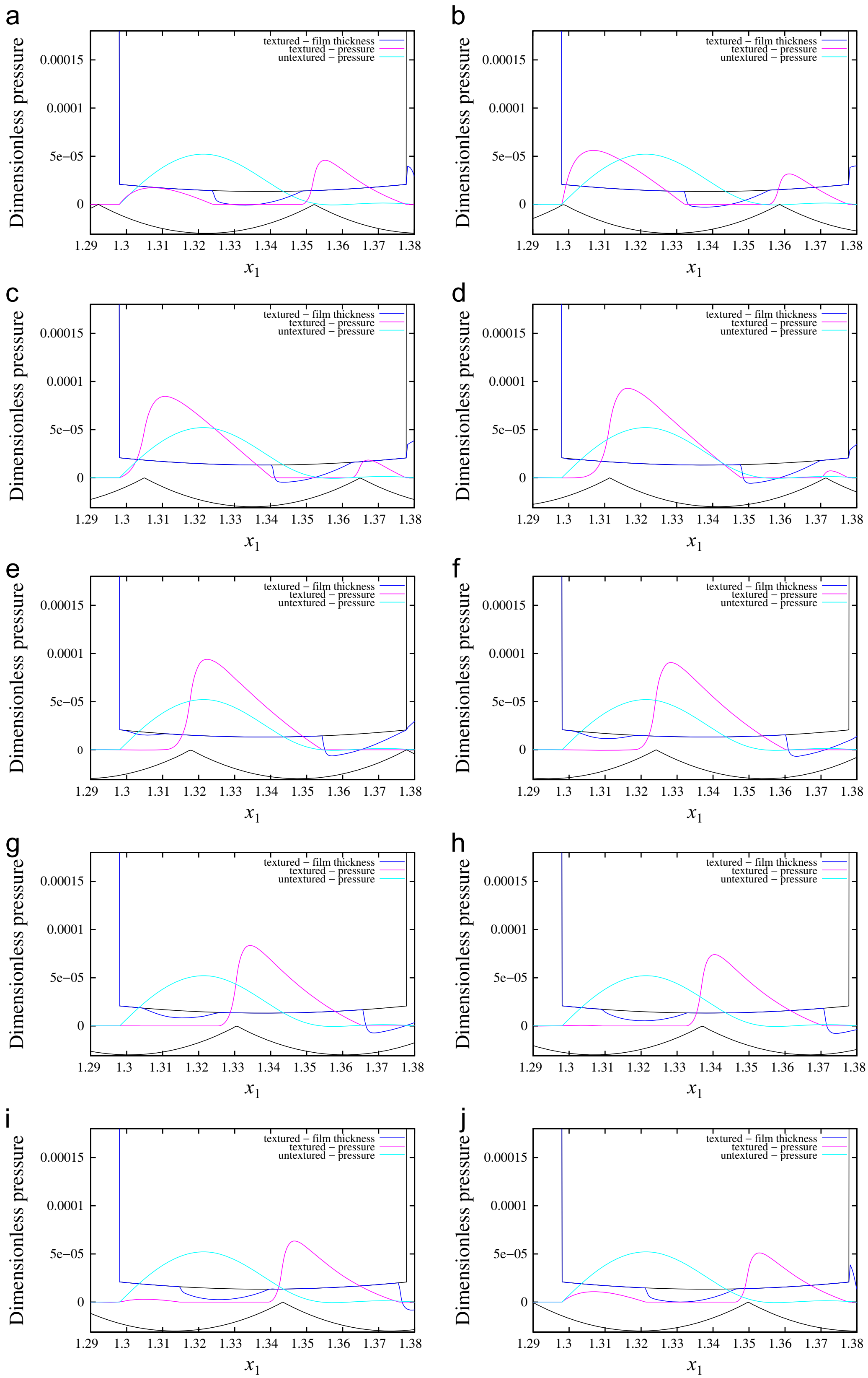

Fig. 10. Instantaneous pressure and film thickness profiles for Case III at times: (a) $t=0.9920$, (b) $t=0.9984$, (c) $t=1.0048$, (d) $t=1.0112$, (e) $t=1.0176$, (f) $t=1.0240$, (g) $t=1.0304$, (h) $t=1.0368$, (i) $t=1.0432$, (j) $t=1.0496$ (Points “a” through “j” in the insets of Fig. 7(e) and (f)).

one it is 5.71. The friction coefficient, in turn, is lower for the textured liner (0.0087) than for the untextured one (0.0101). The instantaneous profiles of pressure and film thickness that are shown in Fig. 10 help understand this apparent paradox. On the right half of each pocket, the diverging geometry generates a vast cavitated zone. In this zone, the saturation variable θ falls below θ_s thus making the Couette contribution to the friction to vanish in this zone.

The pressure generation mechanism that takes place in close-packed square arrays of pockets (such as in Case III) of different radii is shown in Fig. 12. There, the ring position is fixed at $Z=2.5$ μ, and we examine the pressure field (along $x_2 = per/2$) at two different instants for 10-μm-deep pockets of radii 100, 200 and 400 μ. It is clear from the picture that there is a pressurized region along the left part of each pocket, which acts as a texture-cell-level wedge. The pressurized region moves with the pocket but is otherwise quite constant. The peak pressure and the load

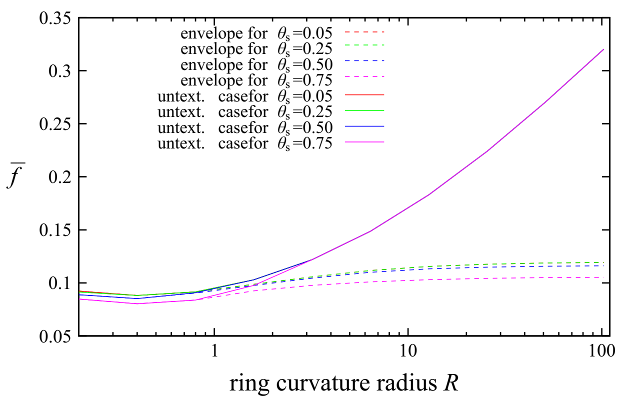

Fig. 11. Lower envelopes of the friction curves as obtained taking different values of θ_s, namely 0.05, 0.25, 0.5 and 0.75. Also shown are their corresponding untextured cases for comparison.

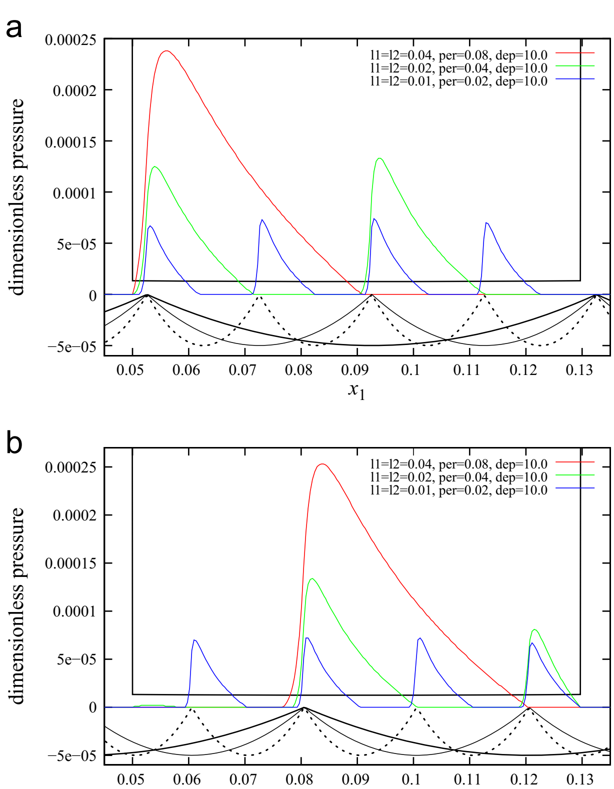

Fig. 12. Pressure profiles with fixed ring position Z=2.5 at time (a) $t=1.092$ and (b) $t=1.200$ (R=51.2).

carrying capacity increase with the pocket size, so that the optimal texture is a close-packed square array of pockets approximately the size of the ring width. The optimal depth as suggested by our study is 10 μ, though it is probably load-dependent.

A remark on the friction model: Above, all computations of the friction coefficient have adopted the model parameter $\theta_s = 0.95$. Similar results are obtained for other values of θ_s. In fact, Fig. 11 shows the lower envelopes of the friction curves for $\theta_s = 0.05$, 0.25, 0.50 and 0.75. All of them are qualitatively consistent with those of $\theta_s = 0.95$, showing that for small-R rings ($R<1.6$) the untextured liner yields minimal friction, while for large-R rings there exist friction-reducing textures.

4. Conclusions

In this paper we have studied the consequences of texturing the liner surface on the tribological performance of the ring/liner contact with a (fixed) load that corresponds to hydrodynamic lubrication conditions. The study is quite fundamental, considering constant relative velocity between the contacting surfaces, and thus the main observations are applicable to other devices, such as thrust bearings and lip seals.

The reported results emerge as a compilation of hundreds of runs, each of which involved a transient dynamically coupled calculation. An efficient and robust numerical methodology allowed such runs to be performed with the mass-conservative model of Elrod and Adams [23] and a realistic mass value for the ring. The results were computed on a mesh with less than 1% discretization error, as shown by a convergence study.

It was observed that the ring profile determines whether pocketing the liner is beneficial or not. The more conformal the contact, the greater the reduction that can be obtained in the friction by texturing the liner with pockets of properly chosen parameters. Up to 73% reduction in the friction coefficient and up to 86% increase in minimum film thickness were numerically obtained.

In fact, for the specific conditions of our study, corresponding to $S=10^{-3}$ and a fully flooded ring with width 800 μ, the texture corresponding to Case III appears as a good choice. It consists of a close-packed square array of circular pockets of radius 300 μ and depth 10 μ.

A liner with this texture would perform, as far as the mathematical model remains valid (see, e.g., [32]), slightly better than an untextured one for a typical compression ring with $R \simeq 5$ cm. Further, the friction when using this textured liner would grow very slowly as the ring undergoes wear (which increases R), much more slowly than with an untextured liner.

It should however be noted that close-packed textures may be structurally fragile, since the walls between pockets are very thin. Physical restrictions on the acceptable textures should be incorporated before choosing an optimal one.

The time-varying conditions of actual ring/liner contacts in internal combustion engines, in which the piston velocity and the load on the rings change along the engine cycle and starved conditions take place at several instants, make the results reported here not directly applicable to the practical selection of a cylinder liner texture. To guide such selection, a broader database (experimental and numerical) encompassing multiple loads and feeding conditions is needed. This is the subject of ongoing work.

Acknowledgements

The authors want to thank FAPESP (São Paulo Research Foundation, Grants 2011/24147-5 and 2012/14481-8) and CNPq (Brazil) for financial support.

References

[1] Holmberg K, Andersson P, Erdemir A. Global energy consumption due to friction in passenger cars. Tribol Int 2012;47:221–34.

[2] Kligerman Y, Etsion I , Shinkarenko A. Improving tribological performance of piston rings by partial surface texturing. J Tribol 2005;127(3):632–8.

[3] Tomanik E. Modelling the hydrodynamic support of cylinder bore and piston rings with laser textured surfaces. Tribol Int 2013;59:90–6.

[4] Gadeschi G, Backhaus K, Knoll G. Numerical analysis of laser-textured piston-rings in the hydrodynamic lubrication regime. J Tribol 2012;134(October) 041702–1–041702–8.

[5] Yin B, Li X, Fu Y, Wang Y. Effect of laser textured dimples on the lubrication performance of cylinder liner in diesel engine. Lubr Sci 2012;24:293–312.

[6] Tanaka H, Ichimaru K. Numerical simulation of oil-film behavior on cylinder liners in sliding contacts with piston rings. Transient Process Tribol 2004:283–90.

[7] Ausas R, Ragot P, Leiva J, Jai G, Bayada M, Buscaglia G. The impact of the Cavitation model in the Analysis of Micro-Textured Lubricated Journal bearings. ASME J Tribol 2009;129:868–75.

[8] Zhang J, Meng Y. Direct observation of cavitation phenomenon and hydrodynamic lubrication analysis of textured surfaces. Tribol Lett 2012;46:147–58.

[9] Wang X, Adachi K, Otsuka K, Kato K. Optimization of the surface texture for silicon carbide sliding in water. Appl Surf Sci 2006;253:1282–6.

[10] Yuan S, Huang W, Wang X. Orientation effects of micro-grooves on sliding surfaces. Tribol Int 2011;44:1047–54.

[11] Qiu Y, Khonsari M. Experimental investigation of tribological performance of laser textured stainless steel rings. Tribol Int 2011;44:635–44.

[12] Kovalchenko A, Ajayi O, Erdemir A, Fenske G, Etsion I. The effect of laser surface texturing on transitions in lubrication regimes during unidirectional sliding contacts. Tribol Int 2005;38:219–25.

[13] Mishra S, Polycarpou A. Tribological studies of unpolished laser surface textures under starved lubrication conditions for use in air-conditioning and refrigeration compressors. Tribol Int 2011;44:1890–901.

[14] Kovalchenko A, Ajayi O, Erdemir A, Fenske G. Friction and wear behavior of laser textured surface under lubricated initial point contact. Wear 2011;271:1719–25.

[15] Ali F, Krupka I, Hartle M. Analytical and experimental investigation of friction of non-conformal point contacts under starved lubrication. Meccanica 2013;48:545–53.

[16] Li J, Zhou F, Wang X. Modify the friction between steel ball and PDMS disk under water lubrication by surface texturing. Meccanica 2011;46:499–507.

[17] Kim B, Chung W, Rhee M, Lee S. Studies on the application of laser surface texturing to improve the tribological performance of AlCrSiN-coated surfaces. Met Mater Int 2012;18(6):1023–7.

[18] Pettersson U, Jacobson S. Influence of surface texture on boundary lubricated sliding contacts. Tribol Int 2003;36:857–64.

[19] Pettersson U, Jacobson S. Textured surfaces for improved lubrication at high pressure and low sliding speed of roller/piston in hydraulic motors. Tribol Int 2007;40:355–9.

[20] Costa H, Hutchings I. Hydrodynamic lubrication of textured steel surfaces under reciprocating sliding conditions. Tribol Int 2007;40:1227–38.

[21] Tomanik E. Friction and wear bench test of different engine liner surface finishes. Tribol Int 2008;41:1032–8.

[22] Grabon W, Pawlus P, Sep J. Tribological characteristics of one-process and two-process cylinder liner honed surfaces under reciprocating sliding conditions. Tribol Int 2010;43:1882–92.

[23] Elrod H, Adams M. A computer program for cavitation, Technical report 190. In: 1st LEEDS LYON symposium on cavitation and related phenomena in lubrication, I.M.E. vol. 103, 1974. p. 354.

[24] Ausas R, Jai M, Ciuperca I, Buscaglia G. Conservative one-dimensional finite volume discretization of a new cavitation model for piston-ring lubrication. Tribol Int 2013;57:54–66.

[25] Braun M, Hannon W. Cavitation formation and modelling for fluid film bearings: a review. J Eng Tribol 2010;224:839–63.

[26] Etsion I. State of the art in laser surface texturing. J Tribol: Trans ASME 2005;127:248–53.

[27] Bayada G, Chambat M. The transition between the Stokes equations and the Reynolds equation: a mathematical proof. Appl Math Optim 1986;14 (1):73–93.

[28] Bayada G, Chambat M, El Alaoui M. Variational formulations and finite element algorithms for cavitation problems. ASME J Tribol 1990;112:398–403.

[29] Ausas R, Jai M, Buscaglia G. A mass-conserving algorithm for dynamical lubrication problems with cavitation. ASME J Tribol 2009;131(031702):7.

[30] Venner CH, Lubrecht AA. Multilevel methods in lubrication. Elsevier Tribology Series, 2000;37.

[31] Smith E. Optimising the design of a piston-ring pack using DoE methods. Tribol Int 2010;44:29–41.

[32] Dobrica M, Fillon M. About the validity of Reynolds equation and inertia effects in textured sliders on infinite width. Proc IMechE 2008;223:69–78.